Collisionless Damping of Localized Plasma Waves in Laser-Produced Plasmas and Application to Stimulated Raman Scattering in Filaments

Stimulated Raman scattering (SRS), an instability that converts laser light incident on a plasma into plasma waves and lower-frequency scattered photons, has been a major concern in laser fusion research for many years. The scattered photons represent wasted energy, and the plasma waves can produce suprathermal electrons that penetrate and preheat the target core, thereby preventing efficient implosion. Interest in SRS has intensified in recent years as experiments with higher laser intensities and longer-scale-length plasmas, intended to simulate laser–plasma interaction conditions in the National Ignition Facility (NIF), have yielded SRS reflectivities as high as 25%.[1] Furthermore, for many years theoretical models of SRS have had difficulty accounting for several aspects of the experimental observations: SRS is often observed at incident intensities well below the theoretical threshold; the spectrum of the scattered light is broader and extends to shorter wavelengths than theory predicts; and anomalous spectral and temporal structure is observed.[2] More recently it has been found that "beam smoothing," which involves small increases in the spatial and/or temporal bandwidth of the incident laser light, effectively suppresses the SRS instability,[3,4] while theory predicts that much larger increases in the bandwidth, comparable to the instability growth rate, would be required for such suppression.

To account for the discrepancies in the threshold and spectrum, it was proposed some time ago[5,6] that SRS is not occurring in the bulk plasma, but rather in intense light filaments formed from hot spots in the incident laser beam by the self-focusing instability. Intensities in such filaments could easily surpass SRS thresholds, even if the average beam intensity was well below the threshold, and the higher intensity would be expected to drive SRS over a broader range of wavelengths. The more recent experimental observations add further support to this hypothesis: Filamentation can be suppressed by much lower bandwidths than would be required to suppress SRS directly, and the anomalous spectral and temporal features may be accounted for by the temporal evolution of the waveguide mode structure in the filament. A thorough discussion of the anomalies in SRS experiments and how they can be explained by filamentation is presented in Afshar-rad *et al*.,[7] along with direct observational evidence for the occurrence of SRS in filaments. It should be pointed out that this interpretation of the experimental observations has great potential significance for NIF since it suggests that the bandwidth already incorporated in the NIF design to improve irradiation uniformity may also be sufficient to suppress or greatly reduce SRS.

The experimental evidence for the connection between filamentation and SRS is especially compelling for the short-wavelength portion of the SRS spectrum. Recently reported experiments[1,3,4] on the Nova laser at LLNL studied a 351-nm laser beam interacting with a preformed plasma at a temperature of ~3 keV. The density profiles of these plasmas have a large central region at densities of about 10% n_{crit} and fairly sharp boundaries. LASNEX simulations of these targets, in concert with the laser interactions postprocessor (LIP),[8] predicted a narrow SRS spectrum at ~600 nm, whereas observations showed a much broader spectrum extending to shorter wavelengths. In some cases without beam smoothing, this part of the spectrum dominated, with a peak near 450 nm. Substantial scattering at these wavelengths requires long regions of very-low-density plasma, which do not appear in the hydrodynamic simulations but could exist in a filament. This part of the spectrum is strongly peaked in the backscatter direction and is greatly diminished by increased bandwidth:[4] further indications that this scattering is associated with filamentation. The beam-deflection phenomenon, observed in many of these experiments and associated with filamentation in theory and simulations,[9,10] provides independent evidence that filamentation is occurring in these plasmas.

One remaining difficulty with this interpretation concerns the damping of SRS at these wavelengths. The parametric nature of the SRS instability requires that the participating electromagnetic and electrostatic waves satisfy frequency- and wave-vector–matching conditions:

$$\omega_0 = \omega + \omega_s, \quad k_0 = k + k_s,$$

where (ω_0,k_0), (ω_s,k_s), and (ω,k) are the frequency and wavenumber pairs of the incident and scattered electromagnetic waves and the plasma wave, respectively. In the fluid approximation the dispersion relations for these three waves are

$$\omega_0^2 = \omega_p^2 + c^2k_0^2,$$
$$\omega_s^2 = \omega_p^2 + c^2k_s^2,$$
$$\omega^2 = \omega_p^2 + 3v_T^2k^2 = \omega_p^2\left(1+3k^2\lambda_D^2\right),$$

where ω_p is the plasma frequency, v_T is the electron thermal velocity, and λ_D is the Debye length. Short-wavelength scattering requires that ω and therefore ω_p be small so that $\omega_s \approx \omega_0$. Consequently, the thermal dispersion term becomes significant, with $k\lambda_D$ of order 1. It is well known that for electrostatic waves in homogeneous plasmas Landau damping becomes very strong when $k\lambda_D \geq 0.4$. This suggests that the plasma wave associated with short-wavelength SRS will be heavily Landau damped, and, in fact, in this case SRS is more properly referred to as stimulated Compton scattering (SCS), which has a much lower growth rate and correspondingly higher threshold; thus, significant scattering would not be expected in this range of wavelengths. One possible explanation, recently proposed by Afeyan *et al.*,[11] is that thermal transport across steep temperature gradients, produced by inverse bremsstrahlung absorption in intense hot spots in the laser beam, produces a modified non-Maxwellian electron distribution function (MDF) in the hot spot with a depleted high-energy tail. Since the high-energy electrons are responsible for Landau damping, this would result in a reduced damping in the hot spots, allowing SRS to occur. The thermal-electron mean free path in these plasmas, however, is typically much larger than the size of the laser hot spots, and the mean free path for the high-energy electrons is even longer, so it is not clear that the required steep gradient in the high-energy electron population could be sustained. Moreover, recent experiments[12] using random phase plates suggest that hot spots alone, without self-focusing, cannot account for the levels of SRS observed.

In this article we propose an alternative explanation. We investigate the collisionless damping of plasma waves propagating in a bounded region of plasma, such as the interior of a filament, and find that it can be much smaller than expected on the basis of the infinite-medium Landau theory, even with a Maxwellian electron distribution. Using a simple model of a filament and its internal modes, we then apply these results to SRS in filaments.

Linear Collisionless Damping of Localized Plasma Waves

SRS occurs when plasma waves originating in noise are amplified by their interaction with the laser field. The initiation and early growth of the instability thus depend on the behavior of small-amplitude plasma waves, so for the purpose of analyzing SRS thresholds and growth rates, a linear treatment of the plasma waves suffices. Furthermore, in the plasmas of interest here, the mean free paths and collision times are much longer than the spatial and temporal scales of interest, so the plasma may be regarded as collisionless. We will therefore be interested in the collisionless damping of localized small-amplitude plasma waves. This process is often referred to as "transit-time damping" since it results from the transfer of energy from the wave to particles transiting the localization volume. Although the analysis presented here is self-contained, we treat transit-time damping in filaments using the method presented in greater generality in an earlier article.[13]

Since we are interested in filaments, we will analyze plasma waves confined in a cylindrical geometry (though the extension to other geometries will be evident and the case of slab geometry is treated in Appendix A). For simplicity, we consider only azimuthally symmetric waveguide modes ($\ell = 0$) for the electromagnetic and electrostatic waves in the cylinder. While self-consistent radial intensity and density profiles for filaments can be calculated numerically,[6] it is adequate for our purposes to consider a simple filament model consisting of a circular cylinder with a sharp boundary at radius R, as shown in Fig. 76.44. The density n_0 inside the filament is assumed to be significantly lower than that outside the filament, so that waveguide modes for the light and plasma waves have negligible fields extending outside the cylinder. Pressure balance is provided by the ponderomotive potential Ψ_0 of the laser light propagating in the filament. The size and intensity of filaments likely to form in laser-produced plasmas and the properties of the corresponding waveguide modes will be discussed further below.

Inside the filament the electron distribution function is

$$f_0(\mathbf{r},\mathbf{v}) = \frac{n_0}{(2\pi)^{3/2}v_T^3}e^{-v^2/2v_T^2},$$

where $v_T^2 = k_BT_0/m$. Consider a phase-space volume element dV containing a group of co-moving particles passing through the filament. We represent the motion of each particle by the motion of its oscillation center, neglecting the oscillation

amplitude of the particle in the laser field as small compared to the length scales over which the fields vary. Since we are taking the equilibrium ponderomotive potential inside the filament to be uniform, the particle trajectories can then be represented as straight lines within the filament, as shown in Fig. 76.44. Each particle thus acquires an energy ΔE in time $\Delta t = 2\sqrt{R^2 - b^2}/v_\perp$, where b is the impact parameter of the particle and $v_\perp$ is the velocity component perpendicular to the cylinder axis. This energy, which may be positive or negative, is acquired as the particle interacts with the plasma wave trapped in the filament. To conceptually simplify the analysis we take this wave to be a standing wave and we assume that the energy removed from the wave by damping is replaced by a driving process, such as SRS, so that the wave has a constant amplitude. Then, since f_0 is even in $\mathbf{v}$, it is clear that the time-reversed process, in which the particles in a time-reversed phase-space element dV^* interact with the filament, acquiring energy $-\Delta E$ in time Δt, is also occurring. Since we are neglecting collisions, phase-space volume is conserved, $|dV^*| = |dV|$, and the net rate at which energy is transferred to the particles associated with dV is

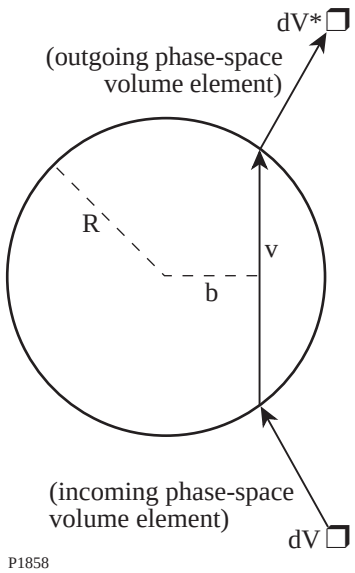

Figure 76.44
Geometry of cylindrical filament model. R is the cylinder radius, v and b are the electron velocity and impact parameter, respectively, and dV denotes a six-dimensional phase-space volume element.

$$\Delta P = \Delta E\left[f_0(E)\,dV - f_0(E+\Delta E)\,dV^*\right]/\Delta t$$

$$\cong -\frac{(\Delta E)^2}{\Delta t}\frac{\partial f_0}{\partial E}\,dV.$$

Integration of this quantity over the phase space within the filament then gives *twice* the collisionless damping rate of the plasma wave since the phase space is effectively included twice in the integration (both forward and backward in time).

First we calculate the energy acquired by a particle interacting with the filament. Inside the filament the potential satisfies the longitudinal plasma-wave dispersion relation, so assuming azimuthal symmetry for simplicity, we can write the potential as

$$\phi(r,z,t) = AJ_0(kr)\,\cos(k_z z + \alpha)\cos(\omega t + \beta), \qquad (1)$$

where A is the infinitesimal wave amplitude, J_0 is the zeroth-order Bessel function, k_z and ω are the axial wave number and frequency of the wave, and α and β are arbitrary constants representing the spatial and temporal phases of the wave, to be averaged over below. The boundary condition is $J_0(kR) = 0$, so k may be any of a discrete set of wave numbers determined by the roots of the Bessel function. We relate ω and k by the fluid plasma dispersion relation

$$\omega^2 = \omega_p^2 + 3\left(k_z^2 + k^2\right)v_T^2.$$

The main kinetic correction to this relation is an imaginary component of ω resulting from the damping we are about to calculate; corrections to the real frequency will result only in a small shift in the resulting SRS spectrum and will be neglected here. Let $t = 0$ be the time when the particle is closest to the cylinder axis. Its change in energy in crossing the filament is then obtained by integrating over the unperturbed orbit:

$$\Delta E = -e\int_{-t_0}^{t_0} \mathbf{v}\cdot\nabla\phi(\mathbf{r},t)\,dt,$$

where $t_0 = \sqrt{R^2 - b^2}/v_\perp$. The total derivative of the potential is

$$\frac{d}{dt}\phi\left[\mathbf{r}(t),t\right] = \mathbf{v}\cdot\nabla\phi\left[\mathbf{r}(t),t\right] + \frac{\partial}{\partial t}\phi\left[\mathbf{r}(t),t\right],$$

so the above integral can be written

$$\Delta E = -e\int_{-t_0}^{t_0}\left\{\frac{d}{dt}\phi\left[\mathbf{r}(t),t\right]-\frac{\partial}{\partial t}\phi\left[\mathbf{r}(t),t\right]\right\}dt.$$

The potential seen by the particle is the same before and after passing through the filament, so

$$\int_{-t_0}^{t_0}\frac{d}{dt}\phi\left[\mathbf{r}(t),t\right]dt = 0$$

and

$$\Delta E = e\int_{-t_0}^{t_0}\frac{\partial}{\partial t}\,\phi\left[\mathbf{r}(t),t\right]dt.$$

Substituting the form of the potential, we have

$$\begin{aligned}\Delta E &= -e\,\omega A\int_{-t_0}^{t_0} J_0\left[kr(t)\right]\cos\left[k_z v_z t+\alpha\right]\sin(\omega t+\beta)dt\\ &= -e\,\omega A\Big\{\cos\alpha\sin\beta\int_{-t_0}^{t_0} J_0\left[kr(t)\right]\cos k_z v_z t\cos\omega t\\ &\qquad -\sin\alpha\cos\beta\int_{-t_0}^{t_0} J_0\left[kr(t)\right]\sin k_z v_z t\sin\omega t dt\Big\}.\end{aligned}$$

Squaring and averaging over the phases α and β gives

$$\left\langle\Delta E^2\right\rangle = \frac{\omega^2 e^2 A^2}{4}\left\{\left[\int_{-t_0}^{t_0} J_0\left[kr(t)\right]\cos k_z v_z t\cos\omega t dt\right]^2 + \left[\int_{-t_0}^{t_0} J_0\left[kr(t)\right]\sin k_z v_z t\sin\omega t dt\right]^2\right\}.$$

Defining the integrals

$$I_\pm \equiv \int_{-t_0}^{t_0} J_0\left[kr\,(t)\right]\cos\left[(\omega\pm k_z v_z)t\right]dt,$$

we have

$$\left\langle\Delta E^2\right\rangle = \frac{\omega^2 e^2 A^2}{8}\left(I_+^2+I_-^2\right) = \frac{\omega^2 e^2 A^2}{4}I_+^2,$$

where the last form follows from the symmetry: $f_0(v_z) = f_0(-v_z)$, so waves propagating in both directions along the axis must be equally damped. Changing the integration variable to $s = kv_\perp t$,

$$\begin{aligned}I_\pm &= \frac{1}{kv_\perp}\int_{-k\sqrt{R^2-b^2}}^{k\sqrt{R^2-b^2}} J_0\left[\sqrt{(kb)^2+s^2}\,\right]\\ &\quad\times\cos\left[\frac{\omega\pm k_z v_z}{kv_\perp}s\right]ds\\ &= \frac{1}{kv_\perp}G\left(kR,kb,\frac{\omega\pm k_z v_z}{kv_\perp}\right),\end{aligned}$$

where we have defined the function

$$G(x,y,z) = \int_{-\sqrt{x^2-y^2}}^{\sqrt{x^2-y^2}} J_0\left(\sqrt{y^2+s^2}\right)\cos(zs)\,ds,$$

which must be evaluated numerically.

Next we must integrate the above expression for $\left\langle\Delta E^2\right\rangle$ over the six-dimensional phase space inside the cylinder. Note that it depends on the particle coordinates and velocities only through the two quantities kb and $w_\pm \equiv (\omega\pm k_z v_z)/kv_\perp$. The total power being transferred to particles in a length L of filament is

$$\begin{aligned}P &= \int_0^L dz\int_{-\infty}^{\infty}dv_z\int_0^\infty dv_\perp v_\perp\\ &\quad\times\int_0^R dr\,r\int_0^{2\pi}d\theta_r\int_0^{2\pi}d\theta_v\left[-\frac{1}{2}\frac{\left\langle\Delta E^2\right\rangle}{\Delta t}\frac{\partial f_0}{\partial E}\right],\end{aligned}\qquad(2)$$

where the factor 1/2 in the integrand compensates for the double-counting of phase space, as noted above. Because of the rotational symmetry, all particle orbits with the same impact parameter b and speed $|v|$ must make the same contribution to $\left\langle\Delta E^2\right\rangle$, so the quantity in square brackets in (2) depends on r, θ_r, and θ_v only through the impact parameter b. We can therefore transform the last three integrals in the above expression to a single integral over b. First we transform the angles θ_r and θ_v to

$$\begin{aligned}\theta_+ &\equiv \theta_v+\theta_r,\\ \theta_- &\equiv \theta_v-\theta_r.\end{aligned}$$

By shifting portions of the region of angular integration by 2π in θ_r or θ_v, the integral over $[0, 2\pi]$ in θ_r and θ_v becomes an integral over $[0, 4\pi]$ in θ_+ and $[-\pi,\pi]$ in θ_-, as shown in

Fig. 76.45(a). Using the Jacobian $\partial(\theta_r,\theta_v)/\partial(\theta_+,\theta_-)=1/2$, we see that the angular integration is transformed as

$$\int_0^{2\pi} d\theta_r \int_0^{2\pi} d\theta_v \to \frac{1}{2}\int_0^{4\pi} d\theta_+ \int_{-\pi}^{\pi} d\theta_- .$$

Next we use

$$\theta_- = \sin^{-1}\frac{b}{r}, \quad \frac{\partial\theta_-}{\partial b} = \frac{1}{\sqrt{r^2-b^2}}, \quad \text{for } 0 \le \theta_- \le \frac{\pi}{2}.$$

As shown in Fig. 76.45(b), there are four values of θ_- in $[-\pi, \pi]$ for each value of r and b. Because of the cylindrical symmetry these values of θ_- are all physically equivalent, so we can combine the above results to obtain the transformation

$$\int_0^{2\pi} d\theta_r \int_0^{2\pi} d\theta_v \int_0^R dr\, r$$

$$\to 4\cdot\frac{1}{2}\int_0^{4\pi} d\theta_+ \int_0^R db \int_b^R dr\, r \frac{1}{\sqrt{r^2-b^2}}$$

$$\to 8\pi\int_0^R db\sqrt{R^2-b^2}\,.$$

After this transformation, the expression for the power is

$$P = 4\pi L\int_{-\infty}^{\infty} dv_z \int_0^{\infty} dv_\perp v_\perp \int_0^R db$$

$$\times\sqrt{R^2-b^2}\left[-\frac{\langle\Delta E^2\rangle}{\Delta t}\frac{\partial f_0}{\partial E}\right], \qquad (3)$$

where we have done the z-integral using the fact that $\langle\Delta E^2\rangle$ is independent of z.

Using

$$\frac{\partial f_0}{\partial E} = -\frac{n_0}{(2\pi)^{3/2} m v_T^5} e^{-v^2/2v_T^2}, \qquad \Delta t = \frac{2\sqrt{R^2-b^2}}{v_\perp},$$

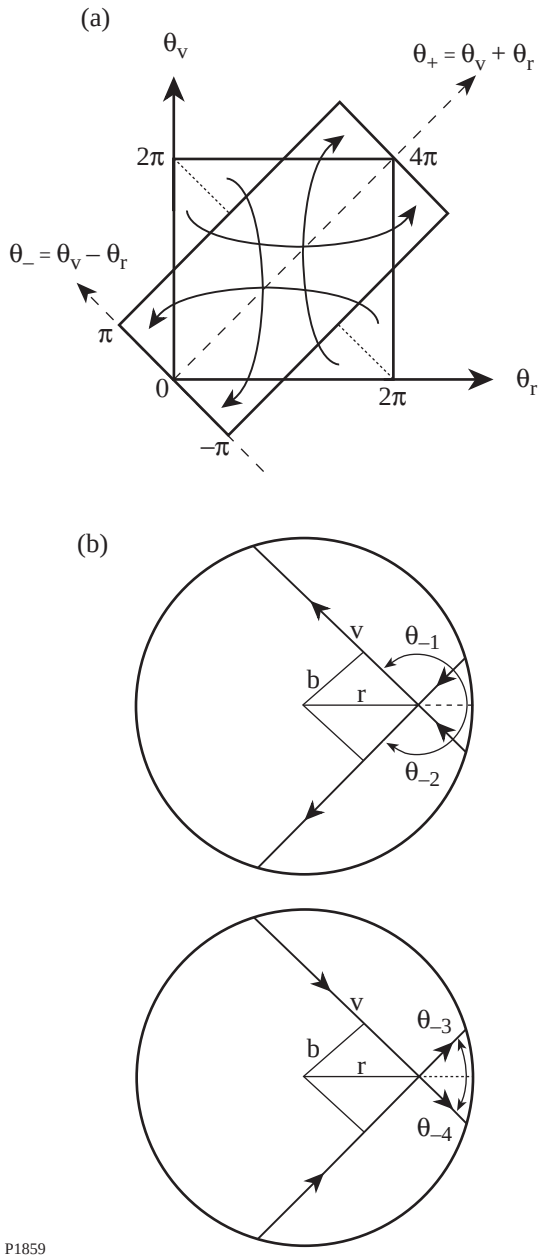

Figure 76.45
Illustration of variable and range transformations used in converting the integral in Eq. (2) to the form in Eq. (3). The angles θ_i in (b) are measured from the dashed extension of r.

and

$$\langle\Delta E^2\rangle = \frac{\omega^2 e^2 A^2}{4k^2 v_\perp^2} G^2\left(kR, kb, \frac{\omega + k_z v_z}{k v_\perp}\right),$$

this becomes

$$P = \frac{n_0 \omega^2 e^2 A^2 L}{4(2\pi)^{1/2} m v_T^5 k^2}$$

$$\times \int_{-\infty}^{\infty} dv_z \int_0^{\infty} dv_\perp \int_0^R db G^2\left(kR, kb, \frac{\omega + k_z v_z}{k v_\perp}\right) e^{-v^2/2v_T^2}.$$

As an aside, we now verify that the above expression gives the familiar result for Landau damping of a plane electrostatic wave as $R \to \infty$. This result can be established in full generality (including finite radial and azimuthal wave numbers) by methods analogous to those employed for slab and spherical geometries in Ref. 14, but the analysis is fairly complex. Since we are interested here in the application to SRS backscatter, we can simplify matters by considering only the special case where the $R \to \infty$ limit is a plane wave with wave number k_z propagating in the z direction ($k = 0$). To simplify the calculation, we take the limit $k \to \infty$ first, and then let $R \to \infty$, so that the cylinder contains a plane wavefront for all $r < R$. This means the boundary conditions will not be satisfied as we take this limit, but this doesn't affect the result since the boundary's contribution to the damping vanishes as it recedes to infinity. For small x, y we have

$$G(x, y, z) \cong \int_{-\sqrt{x^2 - y^2}}^{\sqrt{x^2 - y^2}} \cos z s ds = \frac{2}{z} \sin\left(\sqrt{x^2 - y^2}\, z\right),$$

so

$$\lim_{k \to 0} \frac{1}{k^2} G^2\left(kR, kb, \frac{\omega + k_z v_z}{k v_\perp}\right)$$

$$= \frac{4 v_\perp^2}{(\omega + k_z v_z)^2} \sin^2\left[\frac{\sqrt{R^2 - b^2}}{v_\perp}(\omega + k_z v_z)\right].$$

Now the quantity $\sqrt{R^2 - b^2}/v_\perp$ in the argument of the sine function above is half the time a particle spends in the cylinder; it becomes large as R becomes large, except for the relatively small number of particles that just graze the boundary of the cylinder. Since the relative contribution of the boundary becomes insignificant as $R \to \infty$, we may regard $\sqrt{R^2 - b^2}/v_\perp$ as large for all particles of interest. With this assumption, and using

$$\lim_{\alpha \to \infty} \frac{\sin^2 \alpha x}{\alpha x^2} = \pi \delta(x) \text{ with } \alpha = \sqrt{R^2 - b^2}\ v_\perp,$$

we have

$$\lim_{k \to 0} \frac{1}{k^2} G^2\left(kR, kb, \frac{\omega + k_z v_z}{k v_\perp}\right)$$

$$= \frac{4\pi \sqrt{R^2 - b^2}}{k_z} v_\perp \delta\left(v_z + \frac{\omega}{k_z}\right),$$

so that

$$P = \frac{4\pi n_0 \omega^2 e^2 A^2 L}{4(2\pi)^{1/2} m v_T^5 k_z}$$

$$\times \int_0^{\infty} dv_\perp v_\perp \int_0^R db \sqrt{R^2 - b^2}$$

$$\times \int_{-\infty}^{\infty} dv_z \delta\left(v_z + \frac{\omega}{k_z}\right) e^{-v^2/2v_T^2}$$

$$= \frac{\omega_p^2 \omega^2 A^2 L}{4(2\pi)^{1/2} v_T^5 k_z} e^{-\frac{\omega^2}{2k_z^2 v_T^2}}$$

$$\times \int_0^{\infty} dv_\perp v_\perp e^{-v_\perp^2/2v_T^2} \int_0^R db \sqrt{R^2 - b^2}$$

$$= \frac{\omega_p^2 \omega^2 A^2 L}{4(2\pi)^{1/2} v_T^3 k_z} \frac{\pi R^2}{4} e^{-\frac{\omega^2}{2k_z^2 v_T^2}}.$$

The energy density in a traveling electrostatic plasma wave $E_0 \cos(kx - \omega t)$ is $E_0^2/8\pi$; superimposing two such waves to give a standing wave doubles the amplitude and the energy, so the energy density in a standing wave $E_0 \cos kx \cos \omega t$ is $E_0^2/16\pi$. In our case, $E_{\max} = k_z A$, so the wave energy in a portion of a cylinder of radius R and length L is

$$W = \frac{1}{16} k_z^2 R^2 L A^2 ,$$

and the amplitude damping rate γ of a plane plasma wave is then given by

$$\frac{\gamma}{\omega} = \frac{1}{2}\frac{P}{\omega W} = \sqrt{\frac{\pi}{8}}\frac{\omega_p^2 \omega}{k_z^3 v_T^3} e^{-\frac{\omega^2}{2k_z^2 v_T^2}} ,$$

in agreement with the usual expression for Landau damping.[14]

Returning to the finite radius problem, we can perform one more integration analytically by transforming variables

$$v_z, v_\perp \to u, w,$$

where

$$u = \sqrt{\frac{k}{k_z}} v_\perp , \qquad w = \frac{\omega + k_z v_z}{k v_\perp}, \qquad v_\perp = \sqrt{\frac{k_z}{k}} u,$$

$$v_z = \sqrt{\frac{k}{k_z}} uw - \frac{\omega}{k_z}, \qquad \frac{\partial(v_z, v_\perp)}{\partial(u, w)} = u,$$

and

$$v^2 = \left(\frac{k_z}{k} + \frac{k}{k_z} w^2\right) u^2 - 2\frac{\omega}{k_z}\sqrt{\frac{k}{k_z}} wu + \frac{\omega^2}{k_z^2},$$

and then

$$P = \frac{n_0 \omega^2 e^2 A^2 L}{4(2\pi)^{1/2} m v_T^5 k^2} e^{-\frac{\omega^2}{2v_T^2 k_z^2}}$$

$$\times \int_0^R db \int_{-\infty}^{\infty} dw G^2(kR, kb, w) \int_0^{\infty} duue^{-\beta u^2 - \gamma u} ,$$

where

$$\beta = \frac{1}{2v_T^2}\left(\frac{k_z}{k} + \frac{k}{k_z} w^2\right), \quad \gamma = -\frac{\omega}{k_z v_T^2}\sqrt{\frac{k}{k_z}} w .$$

The integral over u can be carried out using the identity[15]

$$\int_0^{\infty} duue^{-\beta u^2 - \gamma u} = \frac{1}{2\beta} e^{\frac{\gamma^2}{8\beta}} D_{-2}\left(\frac{\gamma}{\sqrt{2\beta}}\right),$$

where D is the parabolic cylinder function, which in this case can be expressed in terms of the error function Φ using

$$D_{-2}(z) = e^{\frac{z^2}{4}}\sqrt{\frac{\pi}{2}}\left\{\sqrt{\frac{2}{\pi}} e^{-\frac{z^2}{2}} - z\left[1 - \Phi\left(\frac{z}{\sqrt{2}}\right)\right]\right\}.$$

The remaining integrations must be carried out numerically; for this purpose it is convenient to make the integration limits finite by changing the integration variable w to ζ:

$$\zeta = \frac{\gamma}{\sqrt{2\beta}} = -\frac{\omega / k_z v_T}{\sqrt{\frac{k_z^2}{k^2} + w^2}} w,$$

$$w = -\frac{k_z}{k}\frac{\zeta}{\sqrt{\omega^2 / k_z^2 v_T^2 - \zeta^2}} .$$

Then we have

$$dw = -\frac{k_z}{k}\frac{\omega^2 / k_z^2 v_T^2}{\left(\omega^2 / k_z^2 v_T^2 - \zeta^2\right)^{3/2}} d\zeta ,$$

$$\frac{1}{2\beta} = v_T^2 \frac{k}{k_z}\left(1 - \frac{k_z^2 v_T^2}{\omega^2}\zeta^2\right).$$

Combining these results with the above expression for P and letting $x = kb$ gives

$$P = CI\left(kR, \frac{\omega}{k_z v_T}\right),$$

where

$$C = \frac{n_0 \omega^2 e^2 A^2 L}{8 m k^3 v_T^3} e^{-\frac{\omega^2}{2k_z^2 v_T^2}}$$

and

$$I\left(kR,\frac{\omega}{k_z v_T}\right)=\int_0^{kR}dx\int_{-\frac{\omega}{k_z v_T}}^{\frac{\omega}{k_z v_T}}d\zeta$$

$$\times\frac{\sqrt{\frac{2}{\pi}}-\zeta e^{\zeta^2}\left[1-\Phi\left(\frac{\zeta}{\sqrt{2}}\right)\right]}{\left(\frac{\omega^2}{k_z^2 v_T^2}-\zeta^2\right)^{1/2}}G^2\left[kR,x,w(\zeta)\right].$$

The average energy density of the plasma waves in the cylinder is

$$\left\langle\frac{E^2}{4\pi}\right\rangle_{t,z}=\frac{1}{4\pi}\left\langle(\nabla\phi)^2\right\rangle_{t,z}$$

$$=\frac{A^2}{16\pi}\left[k^2J_0'^2(kr)+k_z^2J_0^2(kr)\right],$$

so the energy in a length L of the cylinder is

$$W=\frac{1}{8}LA^2\int_0^R r\left[k^2J_0'^2(kr)+k_z^2J_0^2(kr)\right]dr.$$

Using

$$\int sJ_n^2(s)\,ds=\frac{s^2}{2}\left[J_n^2(s)-J_{n-1}(s)J_{n+1}(s)\right],$$

$$J_0'(s)=J_{-1}(s)=-J_1(s),$$

and the boundary condition $J_0(kR)=0$, we have

$$W=\frac{A^2L}{16}\left(\frac{k_z^2}{k^2}+1\right)(kR)^2J_1^2(kR);$$

thus, the amplitude damping rate is given by

$$\frac{\gamma}{\omega}=\frac{1}{2}\frac{P}{\omega W}=\frac{1}{4\pi}\frac{\omega_p^2\omega}{\left(\frac{k_z^2}{k^2}+1\right)k^3v_T^3(kR)^2J_1^2(kR)}$$

$$\times e^{-\frac{\omega^2}{2k_z^2v_T^2}}I\left(kR,\frac{\omega}{k_z v_T}\right).$$

In terms of the plane-wave Landau result given above, this is

$$\frac{\gamma}{\omega}=\left(\frac{\gamma}{\omega}\right)_{\text{Landau}}$$

$$\times\frac{1}{\sqrt{2\pi^3}}\frac{k_z/k}{1+k^2/k_z^2}\frac{1}{(kR)^2J_1^2(kR)}I\left(kR,\frac{\omega}{k_z v_T}\right).\qquad(4)$$

Stimulated Raman Scattering in Filaments

In this section we analyze SRS in filaments using the simple sharp-boundary cylindrical model of the previous section (Fig. 76.44). We determine the filament parameters (radius, etc.) most likely to produce short-wavelength SRS and then estimate the collisionless damping in these filaments using the results of the previous section.

We assume that the pump and backscattered electromagnetic waves propagate as waveguide modes in the filament, so their dispersion relations can be written

$$\omega_0^2=\omega_p^2+c^2\left(k_{0r}^2+k_{0z}^2\right),\qquad(5)$$

$$\omega_s^2=\omega_p^2+c^2\left(k_{sr}^2+k_{sz}^2\right),\qquad(6)$$

where the subscripts r and z denote the radial and axial wave numbers and the boundary conditions require $J_0\left(k_{0r}R\right)=J_0\left(k_{sr}R\right)=0$, where R is the filament radius. The ponderomotive force arising from the beating of the pump and scattered waves drives an electrostatic plasma response. We assume that this response is largest when the frequency and wave numbers of the plasma wave satisfy the fluid dispersion relation

$$\omega^2 = \omega_p^2 + 3v_T^2\left(k_r^2 + k_z^2\right), \tag{7}$$

where again $J_0\left(k_r R\right) = 0$. This approximation will be good as long as the damping rate is much smaller than the frequency ω. As in the previous section, we assume that the SRS process is near threshold, i.e., the pump replaces the energy lost to damping of the scattered waves, so that the frequencies and wave numbers of all the modes can be taken as real. Then the frequencies and axial wave vectors satisfy the matching conditions

$$\omega_0 = \omega_s + \omega\,, \tag{8}$$

$$k_{0z} = k_{sz} + k_z\,. \tag{9}$$

Coupling between the modes is strongest for the lowest-order (smallest radial wave number) modes;[6] since in this simple model all modes have the same boundary condition $J_0\left(k_{0r}R\right) = J_0\left(k_{sr}R\right) = J_0\left(k_r R\right) = 0$, the strongest coupling is obtained by taking

$$k_{0r} = k_{sr} = k_r = j_{01}/R,$$

where $j_{01} \cong 2.4048$ is the smallest root of J_0.

Light propagates in a waveguide mode in the filament because the density inside the filament, n_0, is lower than that outside, N_0. The difference in plasma pressures inside and outside the filament must be balanced by the ponderomotive force of the light confined in the filament. The required intensity in the filament will be a minimum when the increment in density across the filament boundary is the minimum required to confine the pump wave, or

$$\frac{N_0}{n_c} - \frac{n_0}{n_c} = \frac{c^2 k_{0r}^2}{\omega_0^2}. \tag{10}$$

Since the scattered waves are of lower frequency than the pump, they are also confined to the filament when condition (6) holds.

If we are now given the background temperature T_0, density N_0, and pump wavelength $\lambda_0 = 2\pi c/\omega_0$, Eqs. (5)–(10) are six equations determining the six unknowns $\omega_p^2 = 4\pi n_0 e^2/m$, k_{0z}, k_{sz}, k_z, ω, and R in terms of the scattered-light wavelength $\lambda_s = 2\pi c/\omega_s$. We can solve them numerically to obtain in particular the filament radius and density as a function of SRS wavelength, as shown in Figs. 76.46(a)–76.46(b) for the typical experimental parameters $N_0/n_c = 0.1$, $T_0 = 3$ keV, and λ_0 = 351 nm. The SRS spectrum corresponding to these

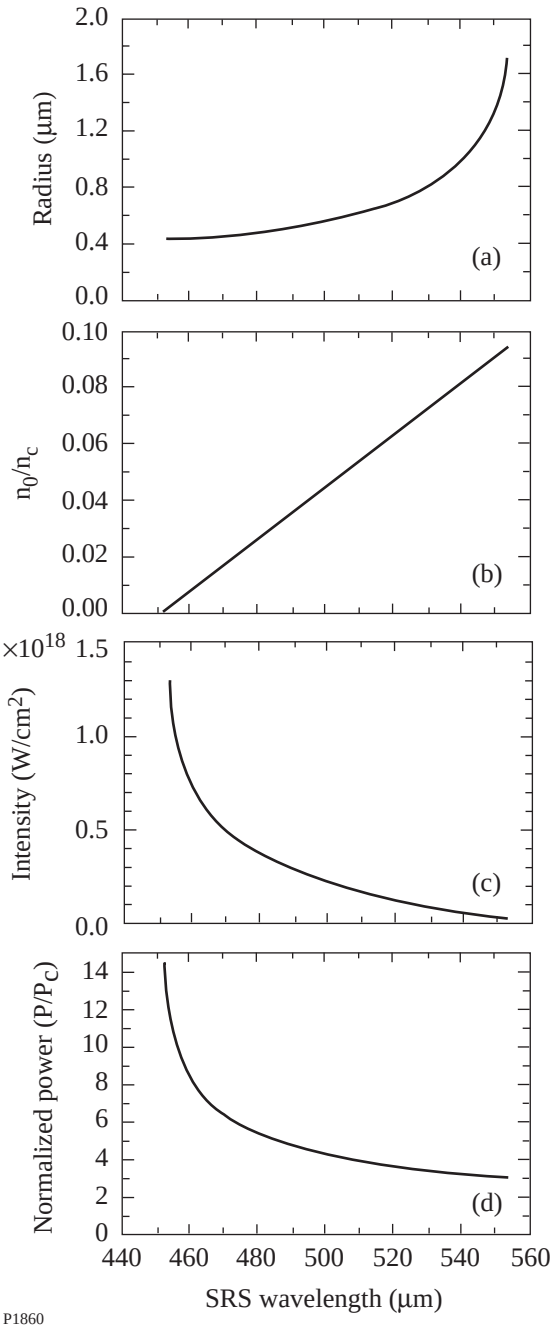

Figure 76.46
Parameters of the filament model as determined in the **Stimulated Raman Scattering in Filaments** section, plotted against the SRS emission wavelength. The filament radius is plotted in (a), the interior density in (b) (for an exterior density of one-tenth critical), the interior light intensity in (c), and the normalized power in the filament in (d).

parameters extends from about 450 nm to about 550 nm. The density plot shows that longer wavelengths would require $N_0/n_c = 0.1$, while shorter wavelengths lead to unphysical negative densities inside the filament. Note that over most of the spectrum the required filament radii tend to be quite small—of the order of a few collisionless skin depths or about a micron for these parameters.

By using the condition that the ponderomotive force balance the difference in plasma pressures inside and outside the filament, we can obtain the intensity and power in the filament. The pressure balance condition is $n_0 = N_0 e^{-v_0^2/4v_T^2}$, where v_0 is the oscillatory velocity of an electron in the electric field of the filament

$$v_0 = eE_{\max}/m\omega_0 \cong 25.6\sqrt{I\left(\mathrm{W/cm^2}\right)}\lambda_0(\mu\mathrm{m})\ \mathrm{cm\ s^{-1}} \qquad (11)$$

with I being the intensity in the filament and λ_0 the laser wavelength. Solving for the intensity yields

$$I\left(\mathrm{W/cm^2}\right) \cong 1.1\times 10^{13}\,\frac{T_0(\mathrm{eV})}{\lambda_0^2(\mu\mathrm{m})}\ln\left(\frac{N_0}{n_0}\right).$$

These intensities are plotted in Fig. 76.46(c). Since in our simplified model the intensity is uniform in the interior of the filament, the power in the filament is obtained by multiplying the intensity by πR^2 and is shown in Fig. 76.46(d) as the normalized power P_N (usually denoted by N in the literature;[16] we use the present notation to avoid confusion with the number density). The normalized power is in general defined by

$$P_N \equiv \frac{e^2}{8\pi m\omega_0^2 T_0}\,\frac{\omega_p^2}{c^2}\iint_A \left|E^2\right| dxdy,$$

where the integration is over the cross-sectional area of the filament.

The normalized power and the filament radius normalized to the collisionless skin depth are useful in comparing our simple filament model with what might be expected of actual filaments. Recently Vidal and Johnston[17] have published some nonlinear simulations of the breakup of laser beams into filaments in plasmas. They find that comparatively long-lived filaments typically tend to form with radii of a few collisionless skin depths and normalized powers P_N in the range of 2 to 15. Larger filaments tend to break up into several smaller filaments within this range; smaller filaments cannot form because of diffraction. From Figs. 76.46(a) and 76.46(d) we see that the filaments our model predicts for short-wavelength SRS have parameters within this range. So we may conclude that, at least in terms of gross parameters such as size and intensity, our model is not an unreasonable representation of the filaments likely to be involved in SRS.

The collisionless damping rate for the plasma mode associated with each SRS wavelength, as calculated in the **Linear Collisionless Damping** section, is shown in Fig. 76.47. For comparison we also show the damping rate for a plasma wave in a homogeneous plasma that would give the same SRS wavelength. Details of the calculation of the damping rate in homogeneous plasmas is given in the Appendix. From Fig. 76.47 we see that for longer wavelengths (corresponding to filaments of large radius) the damping rates approach the homogeneous Landau result, but for shorter wavelengths the smaller radius results in a much-reduced damping as compared to the homogeneous case.

The growth rate for SRS in a filament is readily calculated from the coupled wave equations for the waveguide modes;[6] it is largest when the plasma response is taken to be the fundamental mode (i.e., $k = j_{01}/R$) and is then the same as for a plane-wave pump of the same intensity in a homogeneous plasma. The linear, undamped, homogeneous SRS growth rate γ_0 at high pump intensities is given by[14]

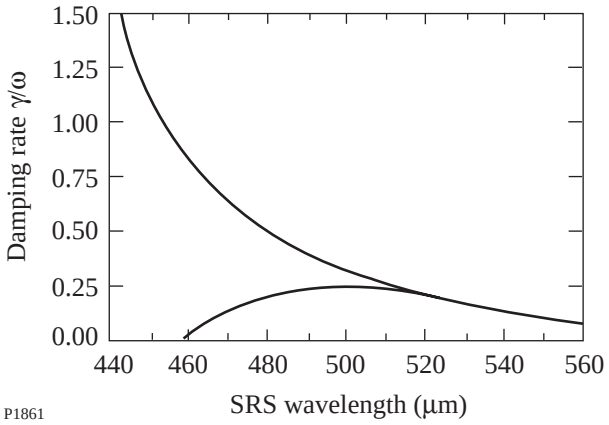

Figure 76.47
Damping rates for plasma waves giving rise to SRS, plotted against the wavelength of the SRS light produced. The upper curve gives the results for a homogeneous plasma, the lower for the filament model in the **Stimulated Raman Scattering in Filaments** section.

$$\frac{\gamma_0}{\omega_0} \cong \sqrt{\frac{\omega_p}{\omega_0}}\,\frac{v_0}{c}.$$

From Fig. 76.46(c) and Eq. (11) we see that $\gamma_0/\omega_0 \approx 0.1$ in the parameter regime of interest to us. This means that the instability will reach nonlinear saturation within a few tens of laser periods temporally and within a few tens of wavelengths spatially, i.e., the spatial and temporal length scales of the SRS interaction are typically much smaller than those of the filament. This justifies the use of an infinitely long, steady-state filament model to study SRS. The high intensities and low damping within the filament also mean that the SRS threshold arising from damping[14]

$$\gamma_0 > \sqrt{\gamma_e \gamma_s}$$

is greatly exceeded, where γ_e and γ_s are the damping rates of the plasma and electromagnetic waves, respectively. Finally, the comparatively low damping of the plasma wave justifies the use of the plasma-wave dispersion relation for the plasma response in these calculations, since for low damping SRS will dominate stimulated Compton scattering.

Conclusions

Discrepancies have long been noted between observations of SRS and theories premised on relatively homogeneous plasmas and uniform laser irradiation. Foremost among these are the onset of SRS at intensities well below the predicted thresholds and the presence of SRS at short wavelengths, which should in theory be suppressed by Landau damping. Many of these discrepancies can be accounted for if the SRS is actually occurring in high-intensity, self-focused light filaments, but this interpretation is still open to the objection that the short-wavelength scattering requires low plasma densities and thus should still be suppressed by Landau damping. We have shown that if short-wavelength SRS is generated in filaments, the Landau damping of the corresponding plasma waves is greatly reduced relative to the damping that would occur if the SRS were being generated outside the filamentary context. This removes the primary objection to the filamentation hypothesis as the explanation for the anomalous SRS observations and suggests that if filamentation is suppressed, for example, by beam-smoothing schemes intended to improve irradiation uniformity, the SRS instability should then be well described by classical theories. One especially important implication of this is that the effective observational threshold for SRS should be significantly increased if filamentation is suppressed by beam smoothing, so that at NIF intensities, for example, SRS would not be significant.

ACKNOWLEDGMENT

This work was supported by the U.S. Department of Energy Office of Inertial Confinement Fusion under Cooperative Agreement No. DE-FC03-92SF19460, the University of Rochester, and the New York State Energy Research and Development Authority. The support of DOE does not constitute an endorsement by DOE of the views expressed in this article.

APPENDIX: Calculation of Collisionless Damping for SRS in Homogeneous Plasmas

For purposes of comparison with our results for the damping of longitudinal waveguide modes in filaments, we also showed in Fig. 76.47 the corresponding damping rates for plane waves in homogeneous plasmas. Since these damping rates are typically much larger and can be comparable to the real frequency, the use of the usual small-damping approximation[14] to Landau damping is not justified. To calculate these damping rates we therefore use the exact expression for the plasma dielectric response function in a Maxwellian plasma:

$$\varepsilon(k,\omega) = 1 + \frac{1}{(k\lambda_D)^2}\left[1 + \Omega Z(\Omega)\right]; \qquad \text{(A1)}$$

where

$$\Omega \equiv \frac{\omega}{\sqrt{2}kv_T} = \frac{1}{\sqrt{2}}\left(1 - \frac{\omega_s}{\omega_0}\right)\left(\frac{n_0}{n_c}\right)^{-\frac{1}{2}}\frac{1}{k\lambda_D}, \qquad \text{(A2)}$$

and where Z denotes the plasma dispersion function,[18] ω_s is the SRS scattered light frequency, n_0 is the homogeneous plasma electron density, v_T is the electron thermal velocity, λ_D is the Debye length, and n_c is the critical density at the laser frequency ω_0. The normal modes are given by the values of k and ω for which $\varepsilon(k,\omega) = 0$. These are the modes that propagate in the absence of a driver, and for a Maxwellian plasma they are damped, i.e., ω has an imaginary component, corresponding to the Landau damping, and the wave amplitude decreases with time. Here, however, we are interested in the steady-state response of a driven plasma wave, corresponding to the situation where SRS is at threshold; i.e., the power provided by the pump wave (the laser beam) exactly compensates for the power lost to damping. (Once above threshold, the instability grows so rapidly that the damping becomes irrelevant.) The plasma response at a given frequency may then be regarded as a driven damped harmonic oscillator, reaching

maximum amplitude at that point in the plasma where $|\varepsilon(k,\omega)|$ is a minimum. SRS can occur at a range of plasma densities below quarter-critical density. Underdense plasmas typically include such a range of plasma densities but are close to isothermal; thus, we regard the temperature as being fixed and look for the values of n_0/n_c and $k\lambda_d$ that minimize $\varepsilon(k,\omega)$. From (A1) and (A2), since ω_s is known, this minimization provides a relation between the two unknowns n_0/n_c and $k\lambda_d$, which we can write by expressing $k\lambda_d$ as a function of n_0/n_c:

$$k\lambda_D\left(\frac{n_0}{n_c}\right) = x \quad \text{such that}$$

$$\left|\varepsilon\left[x,\Omega\left(x,\frac{n_0}{n_c}\right)\right]\right| \le \left|\varepsilon\left[x',\Omega\left(x',\frac{n_0}{n_c}\right)\right]\right| \quad \text{for all } x', \qquad \text{(A3)}$$

where we have used (A2) to represent Ω as a function of $k\lambda_d$ and n_0/n_c.

We obtain another relation between these unknowns from the dispersion relations of the pump and scattered light waves and the frequency and wave-number matching conditions for SRS:

$$\omega_0^2 = \omega_p^2 + c^2k_0^2, \qquad \omega_s^2 = \omega_p^2 + c^2k_s^2;$$
$$\omega = \omega_0 - \omega_s, \qquad k = k_0 - k_s, \quad k_+ = k_0 + k_s,$$

where (ω_0,k_0) and (ω_s,k_s) are the frequency and wave number of the pump and scattered EM waves, respectively. Subtracting the two dispersion relations gives

$$\omega_0^2 - \omega_s^2 = c^2\left(k_0^2 - k_s^2\right) = c^2k_+k, \quad \text{so } k_+ = \frac{\omega_0^2 - \omega_s^2}{c^2k}.$$

Adding the two dispersion relations then yields

$$1 + \frac{\omega_s^2}{\omega_0^2} = 2\frac{n_0}{n_c} + \frac{1}{2}\left[\frac{c^2k^2}{\omega_0^2} + \frac{\left(1-\dfrac{\omega_s^2}{\omega_0^2}\right)^2}{\dfrac{c^2k^2}{\omega_0^2}}\right]. \qquad \text{(A4)}$$

Next we can write

$$\frac{c^2k^2}{\omega_0^2} = \frac{c^2}{v_T^2}\frac{\omega_p^2}{\omega_0^2}\frac{v_T^2k^2}{\omega_p^2} = \left(\frac{v_T^2}{c^2}\right)^{-1}\frac{n_0}{n_c}\left(k\lambda_D\right)^2, \qquad \text{(A5)}$$

and since the temperature, or equivalently v_T, is assumed known, combining (A4) and (A5) gives another relation between $k\lambda_D$ and n_0/n_c, which along with (A3) can be solved numerically to obtain these unknowns and thus determine k. The Landau damping rate, which may also be regarded as the rate of transfer of energy from the wave to the resonant particles, is then given by

$$\frac{\gamma}{\omega} = \frac{1}{2}\,\mathrm{Im}\left[\varepsilon(k,\omega)\right].$$

Using (A1) and the formula for the Z function of a real argument

$$Z(x) = e^{-x^2}\left[i\sqrt{\pi} - 2\int_0^x e^{t^2}\,dt\right],$$

this is

$$\frac{\gamma}{\omega} = \sqrt{\frac{\pi}{8}}\,\frac{\omega_p^2\omega}{k^3v_T^3}\,e^{-\frac{\omega^2}{2k^2v_T^2}}. \qquad \text{(A6)}$$

This is the damping rate for SRS in a homogeneous plasma, as plotted in Fig. 76.47. It should be noted that while (A6) is identical to the Landau damping rate usually obtained for normal modes $\left[\varepsilon(k,\omega) = 0\right]$ under the assumption of weak damping, for driven modes with ω real it is valid even for strong damping.

REFERENCES

1. J. C. Fernández *et al*., Phys. Plasmas **4**, 1849 (1997).
2. A. Simon, W. Seka, L. M. Goldman, and R. W. Short, Phys. Fluids **29**, 1704 (1986), and references therein.
3. B. J. MacGowan *et al*., Phys. Plasmas **3**, 2029 (1996).
4. D. S. Montgomery *et al*., Phys. Plasmas **3**, 1728 (1996).
5. K. Tanaka, L. M. Goldman, W. Seka, M. C. Richardson, J. M. Soures, and E. A. Williams, Phys. Rev. Lett. **48**, 1179 (1982).

6. R. W. Short, W. Seka, and R. Bahr, Phys. Fluids **30**, 3245 (1987), and references therein.

7. T. Afshar-rad *et al*., Phys. Fluids B **4**, 1301 (1992).

8. R. L. Berger, E. A. Williams, and A. Simon, Phys. Fluids B **1**, 414 (1989).

9. R. W. Short, R. Bingham, and E. A. Williams, Phys. Fluids **25**, 2302 (1982).

10. D. E. Hinkel, E. A. Williams, and C. H. Still, Phys. Rev. Lett. **77**, 1298 (1996).

11. B. B. Afeyan, A. E. Chou, J. P. Matte, R. P. J. Town, and W. L. Kruer, Phys. Rev. Lett. **80**, 2322 (1998).

12. C. Labaune *et al*., Phys. Plasmas **5**, 234 (1998).

13. Laboratory for Laser Energetics LLE Review **75**, 200, NTIS document No. DOE/SF/19460-246 (1998). Copies may be obtained from the National Technical Information Service, Springfield, VA 22161.

14. W. L. Kruer, *The Physics of Laser Plasma Interactions*, Frontiers in Physics, Vol. 73, edited by D. Pines (Addison-Wesley, Redwood City, CA, 1988).

15. I. S. Gradshteyn and I. M. Ryzhik, *Table of Integrals, Series, and Products*, edited by A. Jeffrey (Academic Press, New York, 1980), p. 337.

16. J. F. Lam, B. Lippmann, and F. Tappert, Phys. Fluids **20**, 1176 (1977).

17. F. Vidal and T. W. Johnston, Phys. Rev. Lett. **77**, 1282 (1996).

18. B. D. Fried and S. D. Conte, *The Plasma Dispersion Function* (Academic Press, New York, 1961).